

Article

Exploring the Effect of a MnO₂ Coating on the Electrochemical Performance of a Li_{1.2}Mn_{0.54}Ni_{0.13}Co_{0.13}O₂ Cathode Material

Zhong Li *, Peiyue Yang, Zhongxiang Zheng, Qiyun Pan, Yisi Liu, Yao Li and Jinnan Xuan

Institute for Advanced Materials, Hubei Normal University, Huangshi 435002, China; ypy0830@163.com (P.Y.); zzx18370065140@163.com (Z.Z.); qypan@hbnu.edu.cn (Q.P.); yliu88@hbnu.edu.cn (Y.L.); yaoli@hbnu.edu.cn (Y.L.); jnxuan@hbnu.edu.cn (J.X.)

* Correspondence: lizhong99@hbnu.edu.cn

Abstract: The effect of electrochemically active MnO₂ as a coating material on the electrochemical properties of a Li_{1.2}Mn_{0.54}Ni_{0.13}Co_{0.13}O₂ (LTMO) cathode material is explored in this article. The structural analysis indicated that the layered structure of the LTMO was unchanged after the modification with MnO₂. The morphology inspection demonstrated that the rod-like LTMO particles were encapsulated by a compact coating layer. The MnO₂ layer was able to hinder the electrolyte solution from corroding the LTMO particles and optimized the formation of a solid electrolyte interface (SEI). Meanwhile, lithium ions were reversibly inserted into and extracted from MnO₂, which afforded an additional capacity. Compared with the bare LTMO, the MnO₂-coated sample exhibited enhanced electrochemical performance. After the MnO₂ coating, the first discharge capacity rose from 224.2 to 239.1 mAh/g, and the initial irreversible capacity loss declined from 78.2 to 46.0 mAh/g. Meanwhile, the cyclic retention climbed up to 88.2% after 100 cycles at 0.5 C, which was more competitive than that of the bare LTMO with a value of 71.1%. When discharging at a high current density of 2 C, the capacity increased from 100.5 to 136.9 mAh/g after the modification. These investigations may be conducive to the practical application of LTMO in prospective automotive Li-ion batteries.

Keywords: lithium-rich cathode material; surface modification; manganese dioxide; electrochemical performance



Citation: Li, Z.; Yang, P.; Zheng, Z.; Pan, Q.; Liu, Y.; Li, Y.; Xuan, J. Exploring the Effect of a MnO₂ Coating on the Electrochemical Performance of a Li_{1.2}Mn_{0.54}Ni_{0.13}Co_{0.13}O₂ Cathode Material. *Micromachines* **2021**, *12*, 1410. <https://doi.org/10.3390/mi12111410>

Academic Editor: James F. Rusling

Received: 31 October 2021

Accepted: 15 November 2021

Published: 17 November 2021

Publisher's Note: MDPI stays neutral with regard to jurisdictional claims in published maps and institutional affiliations.



Copyright: © 2021 by the authors. Licensee MDPI, Basel, Switzerland. This article is an open access article distributed under the terms and conditions of the Creative Commons Attribution (CC BY) license (<https://creativecommons.org/licenses/by/4.0/>).

1. Introduction

Developing high-energy-density secondary batteries to appease the increasing consumption of electronic apparatuses and electric vehicles is the responsibility of battery researchers [1,2]. In the last two decades, Li-rich Mn-based solid-solution cathode materials of $n\text{Li}_2\text{MnO}_3 \cdot (1-n)\text{LiTMO}_2$ ($0 < n < 1$, TM = Mn, Ni, Co, Mn_{0.5}Ni_{0.5}, Mn_{0.333}Ni_{0.333}Co_{0.333}, etc.) with a layered structure have drawn much attention, which has been ascribed to their outstanding specific capacity [3–5]. The $n\text{Li}_2\text{MnO}_3 \cdot (1-n)\text{LiTMO}_2$ materials are made up of a monoclinic Li₂MnO₃ component (C2/m) and a layered LiTMO₂ component (R-3m) [6,7]. Usually, the two-component notation $n\text{Li}_2\text{MnO}_3 \cdot (1-n)\text{LiTMO}_2$ can be denoted as a layered type of Li_{1+n}TM_{1-n}O₂ [8]. The cutoff voltage of Li_{1+n}TM_{1-n}O₂ is high—up to 4.6–4.8 V—because the Li₂MnO₃ component must undergo an activation over 4.5 V to generate an extra reversible capacity, enabling Li_{1+n}TM_{1-n}O₂ to achieve a much higher specific capacity than that of the LiTMO₂ component [4,9].

As one of the most representative types of Li_{1+n}TM_{1-n}O₂, Li_{1.2}Mn_{0.54}Ni_{0.13}Co_{0.13}O₂ (LTMO, or denoted as 0.5Li₂MnO₃·0.5LiMn_{0.333}Ni_{0.333}Co_{0.333}O₂) can release a competitive capacity of 220–280 mAh/g at 2.0–4.8 V [10–12], and it is considered to be one of the preferred cathode materials for prospective automotive Li-ion batteries. However, LTMO still suffers from several shortcomings that limit its practical application [8–11]. During the first charge, the movement of transition metal ions eliminates oxide ion vacancies generated by the deintercalation of lithium as Li₂O in the Li₂MnO₃ over 4.5 V, which gives rise to a decrease in lithium-ion sites for Li⁺ to be reinserted during the first discharge [3,13].

The reduced insertion of lithium ions, along with the growth of a thick solid electrolyte interface (SEI) layer caused by the side reaction between the LTMO particles and electrolyte, brings about a large initial irreversible capacity loss for the LTMO [4,6]. Meanwhile, the continuous corrosion of the electrolyte on the LTMO surface at a high cut-off voltage of 4.8 V severely deteriorates the cyclic performance [9,14]. Moreover, the LTMO demonstrates an unsatisfied rate capability, which is ascribed to the poor conductivity for the electrons and lithium ions of the Li_2MnO_3 component [7,11].

Currently, many approaches have been implemented to upgrade the electrochemical properties of LTMO, including morphology optimization [15–17], ion doping [18–22], surface coating [10,11,13,14,23–34], and special treatment [35–38]. Among the above-mentioned strategies, modification of the surface of LTMO particles with inert metal oxides has been testified to remarkably enhance the cyclic performance, such as with ZrO_2 [10], TiO_2 [25], Al_2O_3 [23,26], MgO [27], ZnO [28], Pr_6O_{11} [29], and Er_2O_3 [30]. The above chemically stable metal oxides not only stabilize the interface of LTMO particles, but also act as an effective barrier in order to inhibit the etching by the electrolyte [10,23,25–30]. Nevertheless, owing to the electrochemical inertness properties of these metal oxides, the coating layer will reduce the initial specific capacity of LTMO to some extent [10,25–30].

MnO_2 is a well-known electrochemically active oxide that has been widely applied as an active material for the research fields of supercapacitors [39], electrocatalysis [40], and lithium-ion batteries [41]. Recently, the function of MnO_2 has extended to become a surface modification material on cathode materials, such as LiMn_2O_4 [42], $\text{Li}_3\text{V}_2(\text{PO}_4)_3$ [43], and $\text{LiMn}_{0.333}\text{Ni}_{0.333}\text{Co}_{0.333}\text{O}_2$ [44], in order to obtain a better electrochemical performance. Firstly, the stable MnO_2 protective layer can hinder the electrolyte from corroding the cathode particles and can optimize the formation of the SEI layer [42–44]. Furthermore, lithium ions can be inserted into and extracted from the electrochemically active MnO_2 under 3 V, which affords an additional capacity and benefits the Li^+ transfer from the interface of the cathode particle to the electrolyte [44].

Inspired by such research, this article explores the impacts of MnO_2 as a surface modification material on LTMO particles. The structures and morphologies of LTMO before and after MnO_2 modification are thoroughly examined. In addition, the electrochemical properties, such as the specific capacity, initial irreversible capacity loss, cyclic stability, rate capability, and electrochemical impedance spectroscopy, are systematically investigated and discussed.

2. Materials and Methods

2.1. Preparation of Bare LTMO

The bare LTMO cathode material was synthesized as follows: Firstly, stoichiometric amounts of manganese sulfate monohydrate, nickel sulfate hexahydrate, and cobalt sulfate heptahydrate were put into distilled water and stirred continuously to generate a homogeneous solution (1 mol/L). Then, 1 mol/L sodium carbonate solution and 0.3 mol/L ammonium hydroxide were slowly dropped into the above solution. After being stirred at 60 °C for 0.5 h and 30 °C for 12 h, the coprecipitated carbonate precursor was filtered and then rinsed with distilled water. After drying at 80 °C for one day, the filtered powder was thoroughly blended with lithium carbonate, then heated at 500 °C for 5 h and calcined at 900 °C for 15 h in air atmosphere to form LTMO.

2.2. Preparation of MnO_2 -Coated LTMO

The MnO_2 -coated LTMO was prepared as follows: Initially, the LTMO was put into the manganese sulfate solution and stirred vigorously for 0.5 h. Then, an aqueous solution of sodium carbonate was dropped slowly into the above suspension to precipitate manganese carbonate. The obtained slurry was filtered and rinsed with distilled water, subsequently dried at 80 °C for 2 days, and then heated at 400 °C for 2 h in air atmosphere to get the MnO_2 -coated LTMO material with 3 wt % MnO_2 .

2.3. Material Characterization

The materials were characterized by using X-ray diffraction (XRD, D8-Advance, Bruker, Karlsruhe, Baden-Württemberg, Germany) (2θ degree: $10\text{--}70^\circ$, operating rate: $4^\circ/\text{min}$). The particle micro-morphologies were inspected by using field-emission scanning electron microscopy (FESEM, Sirion 200, FEI, Hillsboro, OR, USA), and the elemental distribution was probed with energy-dispersive spectroscopy (EDS, SU8010, HITACHI, Tokyo, Japan). The specific amounts of transition metal ions were determined by using inductively coupled plasma atomic emission spectrometry (ICP-AES, Optima 7000 DV, PerkinElmer, Waltham, MA, USA). The MnO_2 coating layer on the LTMO particles was surveyed by using transmission electron microscopy (TEM, Philips CM12, Philips, Amsterdam, Noord-Holland, Netherlands).

2.4. Electrochemical Evaluations

CR2016 coin cells were fabricated to evaluate the electrochemical properties. To prepare the LTMO (bare and MnO_2 -coated) electrodes, active cathode powder (85 wt %), conductive carbon (10 wt %), and polytetrafluoroethylene (PTFE) (5 wt %) were mixed and continuously rolled to obtain a thin sheet. Subsequently, the thin sheet was separated into several circular films and dried at 120°C in a vacuum to produce the electrodes. The diameter and mass loading of the LTMO (bare and MnO_2 -coated) electrodes were 8 mm and $5\text{--}6\text{ mg}/\text{cm}^2$. The cells were fabricated with the electrodes, metallic lithium sheet, separator (Celgard 2400), and carbonate-based electrolyte (1 mol/L LiPF_6 in the solvents consisting of ethylene carbonate and dimethyl carbonate with the volume ratio of 1:1) under an argon atmosphere. The galvanostatic charge/discharge evaluations were implemented at ambient temperature on an electrochemical test system (CT2001A, Wuhan Land) at 2.0–4.8 V with various current densities (1 C = 250 mA/g). Electrochemical impedance spectroscopy (EIS) was assessed by utilizing a CorrTest electrochemical workstation (frequency: 100,000–0.01 Hz, amplitude: 10 mV).

3. Results and Discussion

3.1. Structures of Bare and MnO_2 -Coated LTMO

The XRD results for the bare and MnO_2 -coated LTMO are exhibited in Figure 1. All of the diffraction peaks (excluding the peaks from 20° to 25°) of both samples belonged to the layered $\text{LiMn}_{0.333}\text{Ni}_{0.333}\text{Co}_{0.333}\text{O}_2$ component with a hexagonal $\alpha\text{-NaFeO}_2$ structure (R-3m) [13]. The weak peaks (020) and (110) located at the degree of $20\text{--}25^\circ$ indicate the existence of the monoclinic Li_2MnO_3 component (C2/m) [27]. The (006)/(012) and (018)/(110) peaks displayed obvious separation in the bare and MnO_2 -coated LTMO, proving the excellence of the layered structure [15,20].

The lattice parameters of the bare and MnO_2 -coated LTMO from XRD patterns are presented in Table 1. Since the ion radii of Ni^+ and Li^+ were very close, cation mixing may have occurred in the preparation process of the materials. If the values of c/a and $I_{(003)}/I_{(104)}$ of 4.96 and 1.2 cannot be achieved, this implies that partial cation mixing exists in a material [16]. Notably, the c/a and $I_{(003)}/I_{(104)}$ of both materials demonstrated values higher than 4.99 and 2.2, respectively, indicating the low degree of cation mixing for the bare and MnO_2 -coated LTMO. Furthermore, no distinct XRD peaks were indexed to MnO_2 in the MnO_2 -coated LTMO, which may have been caused by the low amount and poor crystallinity of MnO_2 [42–44]. The XRD results illustrate that the MnO_2 coating did not damage the lattice structure of the LTMO.

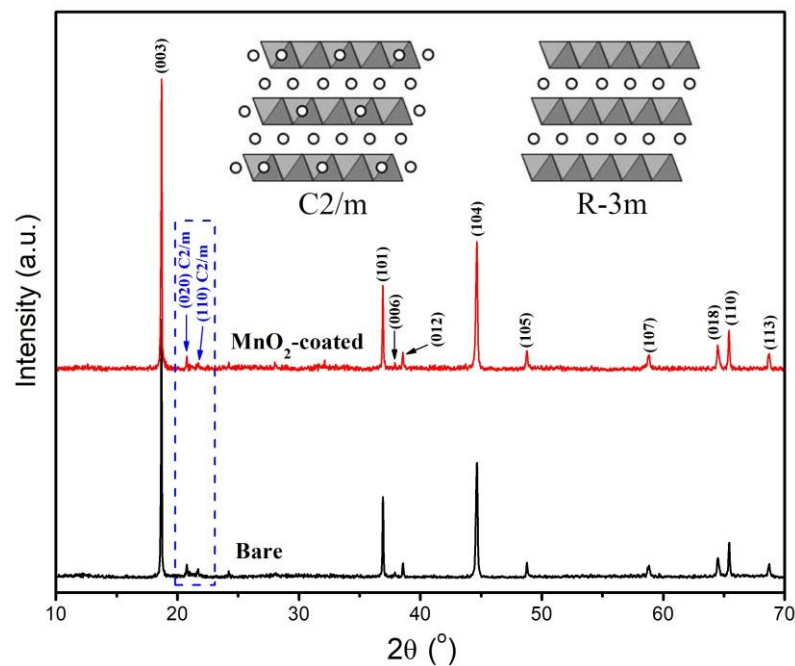


Figure 1. XRD results of bare and MnO₂-coated LTMO.

Table 1. Lattice parameters of the LTMO before and after the MnO₂ modification.

Sample	<i>a</i> (Å)	<i>c</i> (Å)	<i>c/a</i>	<i>I</i> ₍₀₀₃₎ / <i>I</i> ₍₁₀₄₎
Bare	2.8501	14.2384	4.9958	2.24
MnO ₂ -coated	2.8508	14.2364	4.9938	2.26

3.2. Microscopic Morphologies of Bare and MnO₂-Coated LTMO

The field-emission scanning electron microscopy (FESEM) images of the LTMO particles before and after the MnO₂ modification are shown in Figure 2 with different magnifications. The images in Figure 2a,c show that both samples comprised well-crystallized particles, and the particles presented a rod-like morphology with lengths in the range of 300–1000 nm. The bare LTMO particles all displayed clean and smooth surfaces at high magnification (Figure 2b). In contrast, the MnO₂-coated LTMO particles exhibited ambiguous and rough surfaces, which were ascribed to the coarse coating layer (Figure 2d).

The elemental distributions of Mn, Ni, and Co in the bare and MnO₂-coated LTMO particles are shown in Figure 3. For both samples, the transition metal elements were uniformly dispersed in the particles. Moreover, the ICP-AES test was applied to examine the elemental composition of transition metal ions in the two samples, and the measured values are presented in Table 2. The atomic ratio in the bare LTMO was almost identical to the theoretical stoichiometric ratio of Mn, Ni, and Co (0.54:0.13:0.13). It should be noted that the content of the Mn element in the MnO₂-coated LTMO was 3.327%, which was higher than in the bare simple. This result originated from the added MnO₂ coating layer and was very close to the designed amount of the coated Mn element (3 wt %) in this article.

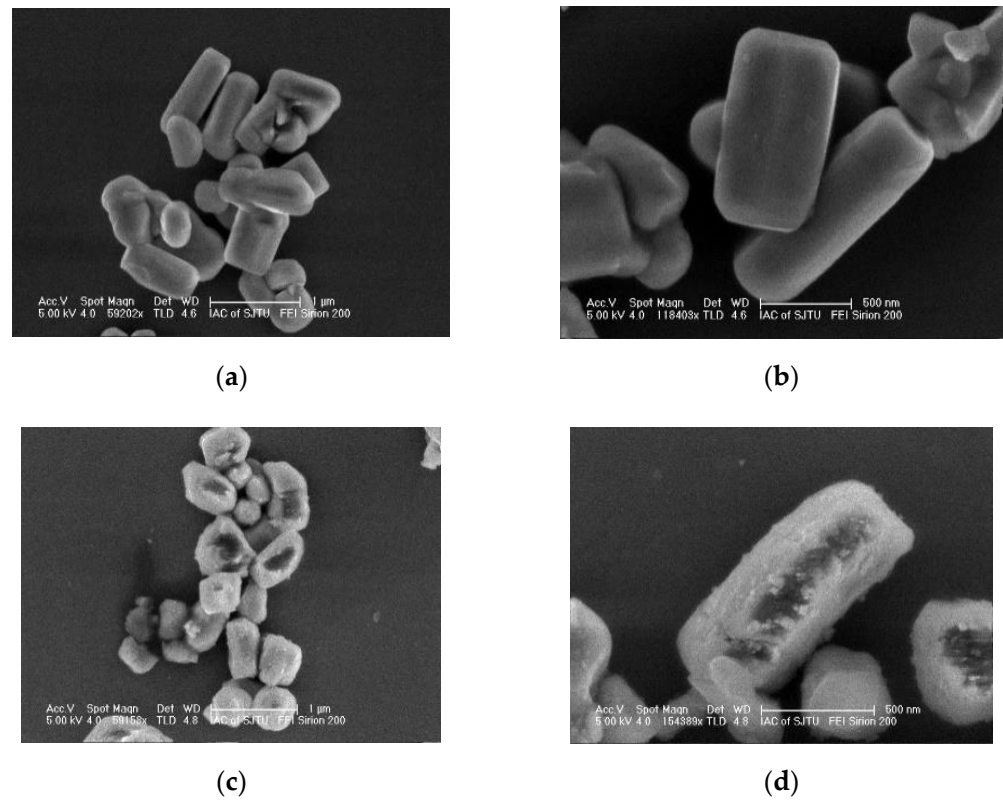


Figure 2. FESEM results for the (a,b) bare and (c,d) MnO₂-coated LTMO particles.

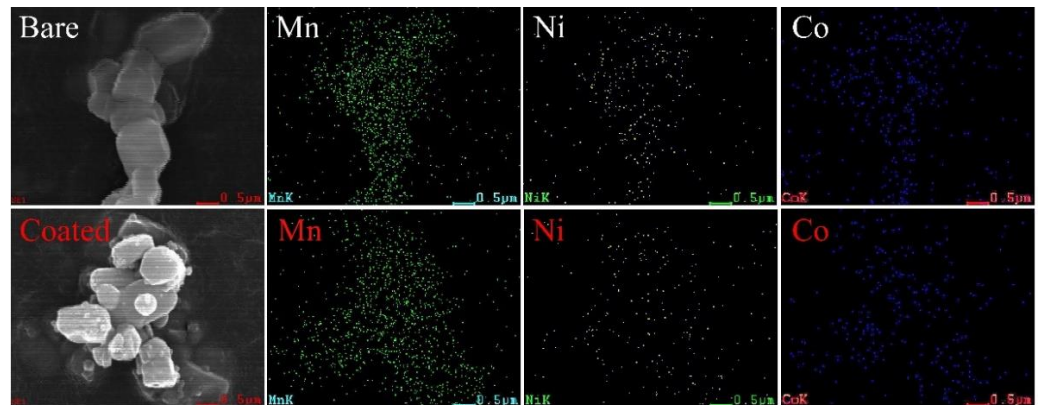


Figure 3. The elemental distributions of Mn, Ni, and Co in the bare and MnO₂-coated LTMO particles.

Table 2. The elemental composition of the bare and MnO₂-coated LTMO determined with ICP-AES.

Sample	Measured Atomic Ratio		
	Mn	Ni	Co
Bare	0.541	0.130	0.129
MnO ₂ -coated	0.559	0.131	0.128

Figure 4 demonstrates TEM images of the bare and MnO₂-coated LTMO particles. Compared to the smooth surface appearing in the bare sample at high magnification (Figure 4b), it can be seen that the MnO₂-coated LTMO in Figure 4d was coated with a compact and distinguishable layer with a thickness from 10 to 50 nm. The compact coated layer was able to encapsulate the LTMO particles to constrain the side reaction and erosion caused by the electrolyte [42–44].

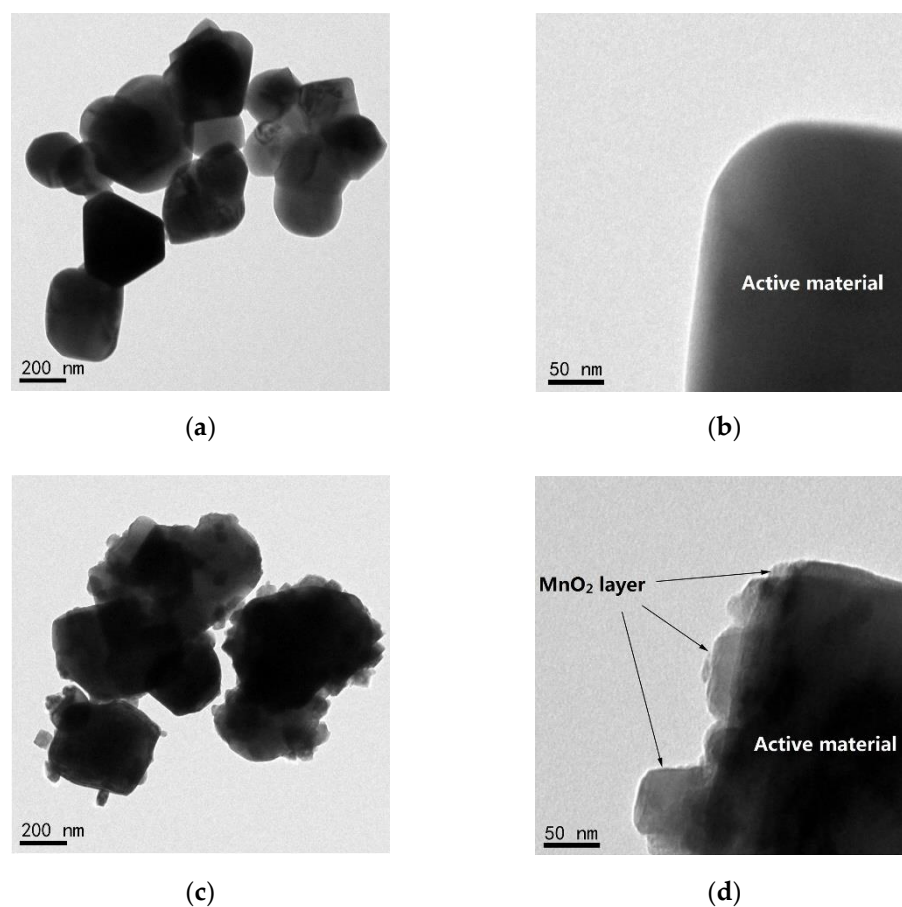


Figure 4. TEM images of the (a,b) bare and (c,d) MnO_2 -coated LTMO particles.

3.3. The Electrochemical Characteristics of Bare and MnO_2 -Coated LTMO at 0.05 C

Figure 5 displays the electrochemical characteristics of the bare and MnO_2 -coated LTMO at 0.05 C for the first two cycles. The first charge curve shows no evident change after MnO_2 coating. Both curves have an inclined plateau at less than 4.5 V and a gentle plateau over 4.5 V (Figure 5a,b), which always appears in LTMO [3,4]. The inclined voltage plateau is derived from the variations of Ni^{2+} to Ni^{4+} , as well as Co^{3+} to Co^{4+} , in the $\text{LiMn}_{0.333}\text{Ni}_{0.333}\text{Co}_{0.333}\text{O}_2$ component [31]. The gentle plateau emerged only in the first charge process, reflecting the activation of the Li_2MnO_3 component, and was accompanied by the removal of Li_2O [3,7,13,17]. As for the first discharge curves, the MnO_2 -coated LTMO exhibited a small potential plateau around 2.8 V, but not in the bare sample. Meanwhile, an additional corresponding charge plateau around 2.9 V occurred in the second charge curve for only the MnO_2 -coated sample.

The dQ/dV profiles for the first two cycles of the LTMO before and after MnO_2 coating are depicted in Figure 5c,d. For the dQ/dV profiles of the bare and MnO_2 -coated LTMO during the initial charge, the anodic peak at 4.0 V was correlated to the inclined plateau in the charge curve (Figure 5a,b), and another peak at 4.5 V was associated with the gentle plateau. Moreover, a cathodic peak at 2.8 V and an anodic peak at 2.9 V appeared in the dQ/dV profiles of the MnO_2 -coated LTMO (Figure 5d), while these two peaks could not be found for the bare sample (Figure 5c), which is in keeping with the information in Figure 5a,b. According to the previous literature [44], these phenomena could stem from the insertion of Li^+ into the coated MnO_2 in the first discharge process and reversible extraction in the following charge process. The results prove that the MnO_2 layer with electrochemical activity was well coated on the surface of the LTMO.

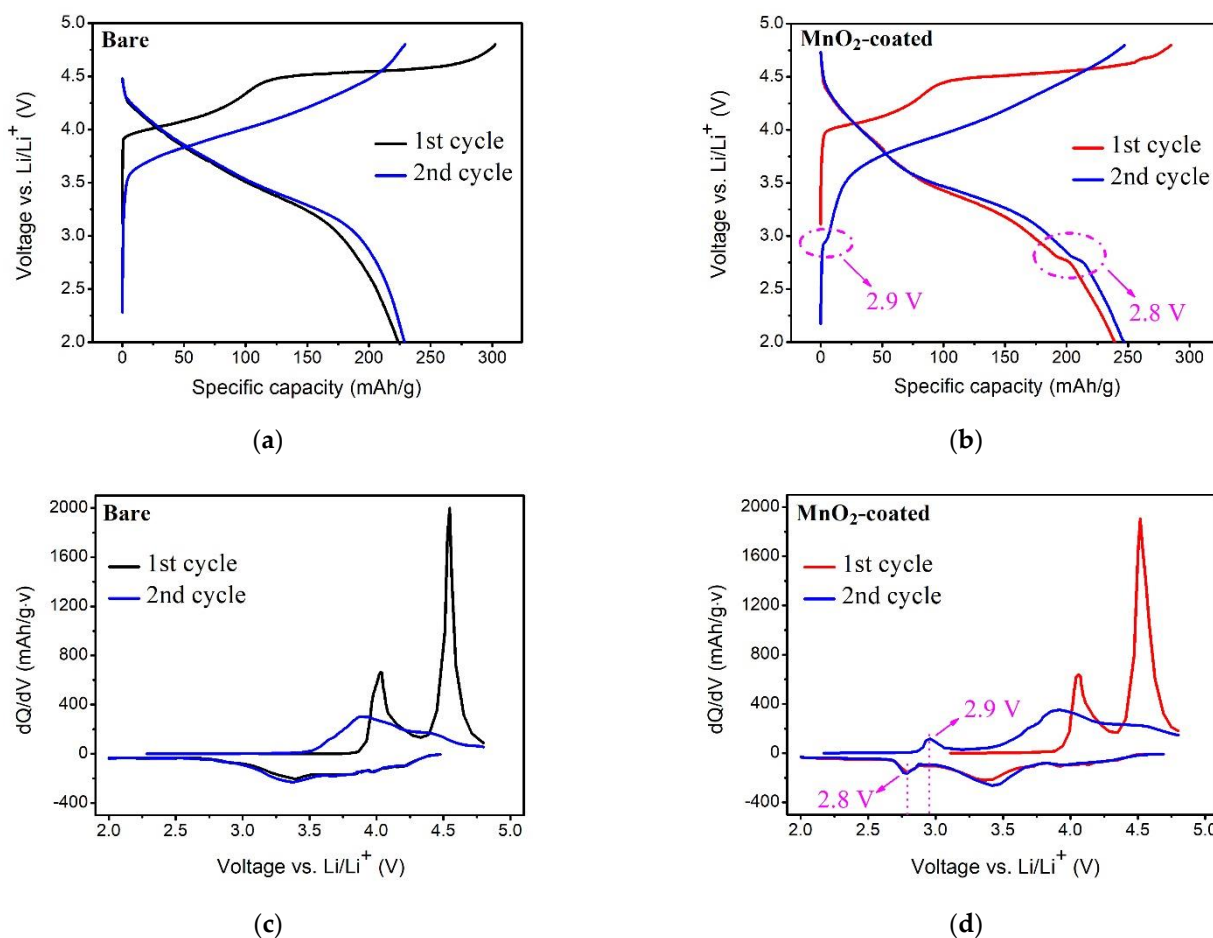


Figure 5. The electrochemical characteristics of the bare and MnO₂-coated LTMO at 0.05 C. (a,b) Charge and discharge curves and (c,d) dQ/dV profiles.

The charge and discharge capacities of the bare LTMO were 302.4 and 224.2 mAh/g, respectively (Figure 5a). In contrast, although the charge capacity of the MnO₂-coated LTMO decreased to 285.1 mAh/g, the discharge capacity climbed up to 239.1 mAh/g (Figure 5b). Consequently, after surface coating, the irreversible capacity loss fell from 78.2 to 46.0 mAh/g, while the coulombic efficiency rose from 74.1% to 83.9%. The electrochemical redox process of the MnO₂ coating layer could be partially responsible for the enhanced first discharge capacity and the reduced initial irreversible capacity loss. Furthermore, the growth of the SEI was reduced, which was ascribed to the repression of the side reaction between the LTMO particles and electrolyte by the MnO₂ modification, which can be another benefit for the promoted electrochemical performance [42–44].

3.4. The Cyclic Performance of Bare and MnO₂-Coated LTMO

Figure 6 displays the cyclic performance of the bare and MnO₂-coated LTMO at 0.5 C for 100 cycles after an activation process at 0.05 C for two cycles. The cyclic performance at 0.5 C of the LTMO cathode was remarkably enhanced after the MnO₂ coating (Figure 6a). Specifically, the bare LTMO delivered 145.6 and 103.5 mAh/g for the first and 100th cycles, and the corresponding retention was 71.1%. In contrast, the MnO₂-coated LTMO released a higher capacity of 181.5 mAh/g at the first cycle and retained 160.1 mAh/g at the end with a retention rate of 88.2%. In addition, the MnO₂-coated sample exhibited less polarization compared to the bare one as the cycle proceeded (Figure 6b,c). Since MnO₂ can hinder the direct contact between the LTMO particles and the electrolyte [42–44], the superior cyclic stability after the surface coating was due to the inhibition of electrolyte corrosion on the surface of LTMO at high potential. Similarly to the metal oxides reported in previous

studies (Table 3), MnO₂ can evidently improve the electrochemical performance of LTMO, and especially has the advantage of reducing the initial irreversible capacity loss.

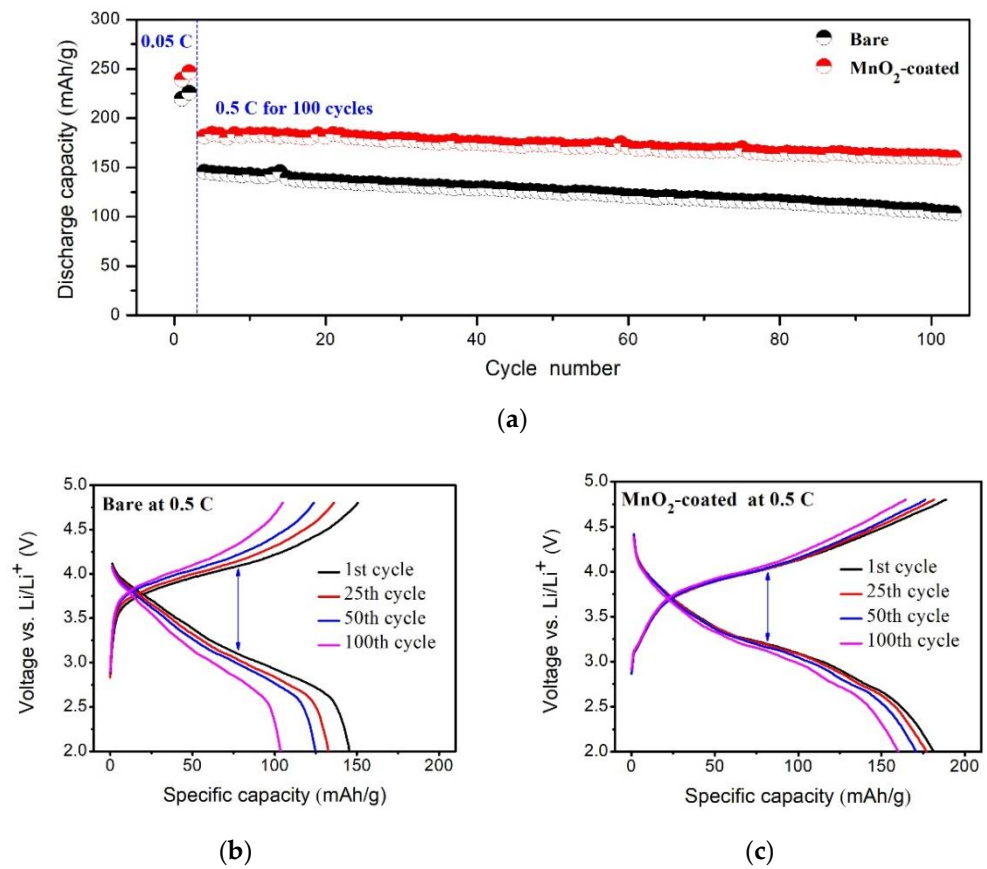


Figure 6. (a) Cyclic performance at 0.5 C. Charge and discharge curves of the (b) bare LTMO and (c) MnO₂-coated LTMO for different cycles.

Table 3. Comparison of the data of MnO₂ with other metal oxides reported as coating materials for LTMO.

Coating Material [References]	Initial Irreversible Capacity Loss (mAh/g)		Cyclic Retention	
	Bare Sample	Coated Sample	Bare Sample	Coated Sample
This work MnO ₂ (3 wt %)	78.2	46	85.4% (50 cycles) 71.1% (100 cycles)	94.3% (50 cycles) 88.2% (100 cycles)
ZrO ₂ (1 wt %) [10]	~70.3	~71.9	87.5% (50 cycles)	94.9% (50 cycles)
Al ₂ O ₃ (3 wt %) [23]	75	41	89.5% (50 cycles)	94% (50 cycles)
TiO ₂ (3 mol %) [25]	75.5	~60	63% (90 cycles)	87% (90 cycles)
MgO (2 wt %) [27]	74.1	73.7	70.7% (100 cycles)	96.4% (100 cycles)
ZnO (20 ALD layers) [28]	77.5	50.8	85.3% (100 cycles)	97.5% (100 cycles)
Pr ₆ O ₁₁ (3 wt %) [29]	73.1	47.8	79.2% (50 cycles)	97.9% (50 cycles)
Er ₂ O ₃ (4 wt %) [30]	64	55	84% (300 cycles)	89% (300 cycles)

3.5. The Rate Capabilities of Bare and MnO₂-Coated LTMO

The bare and MnO₂-coated LTMO were successively tested at 0.05, 0.5, 1, 2, and 0.5 C to evaluate their rate capabilities. As exhibited in Figure 7a, the MnO₂-coated LTMO delivered an elevated capacity in comparison with the bare sample at all C rates. Moreover, as the C rate increased, the discharge midpoint voltage difference between the MnO₂-coated LTMO and the bare LTMO showed an upward tendency (Figure 7b), and the discharge

curves of the bare sample (Figure 7c) exhibited more polarization compared to the MnO_2 -coated sample (Figure 7d). The detailed discharge capacities of the bare LTMO at 0.05, 0.5, 1, and 2 C were 221.7, 143.7, 125.0, and 100.5 mAh/g, respectively. In contrast, the MnO_2 -coated LTMO was able to deliver improved capacities of 242.8, 178.3, 161.8, and 136.9 mAh/g under identical test conditions.

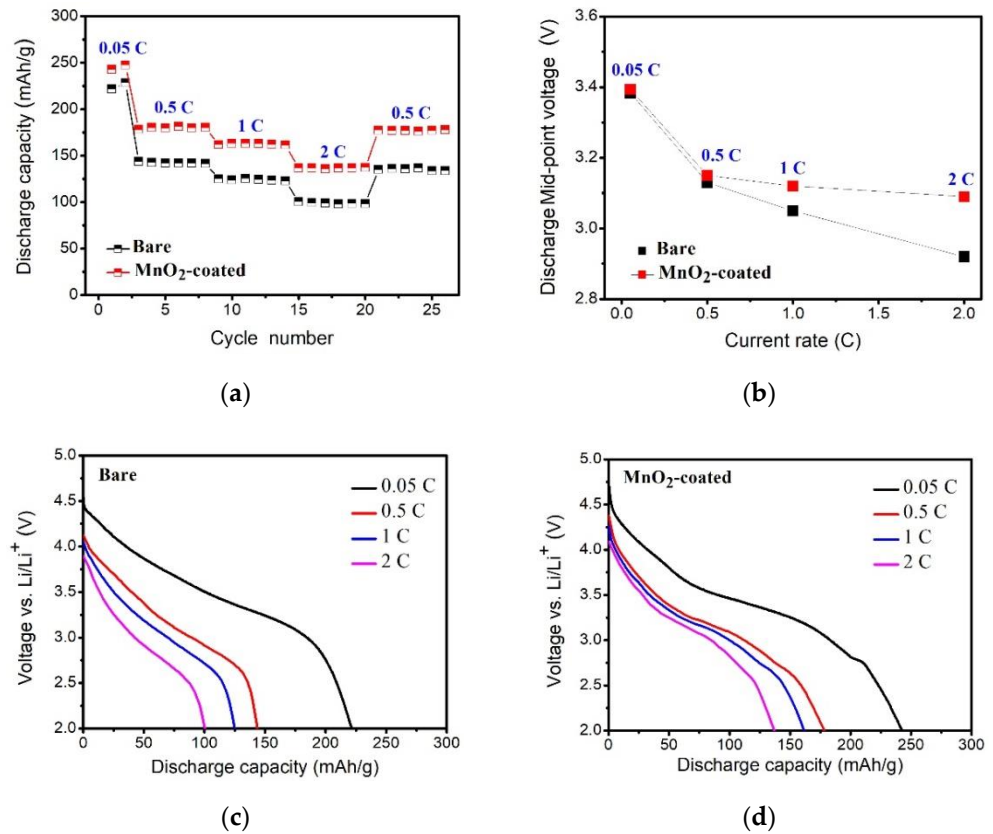


Figure 7. The electrochemical properties of the bare and MnO_2 -coated LTMO evaluated at various C rates. (a) The rate capabilities. (b) The discharge midpoint voltage. (c,d) Discharge curves.

3.6. The EIS Measurements of Bare and MnO_2 -Coated LTMO

To seek the origin of the enhanced electrochemical properties, EIS experiments were conducted on the bare and MnO_2 -coated LTMO. Before the EIS tests, both the bare and MnO_2 -coated samples were charged to 4.6 V after 40 cycles at 0.5 C to achieve an identical status. Figure 8 demonstrates the obtained and fitted Nyquist plots, as well as the equivalent circuit. Similarly, the EIS spectra of the bare and MnO_2 -coated LTMO exhibited a pair of well-defined semicircles and a short, straight line that rose slowly. The intersection between the left side of the initial semicircle and the x -axis reflects the total ohmic resistance (R_s) [45]. The initial semicircle in the high frequency reflects the impedance (R_{sf}) for Li^+ transmission through the interfacial film (SEI layer) of the cathode particle, and the subsequent semicircle in intermediate frequency indicates the resistance of the charge transfer reaction (R_{ct}). The short line in the low frequency is relevant with the Warburg impedance (Z_w), which reflects Li^+ diffusion inside the cathode particles [28,46].

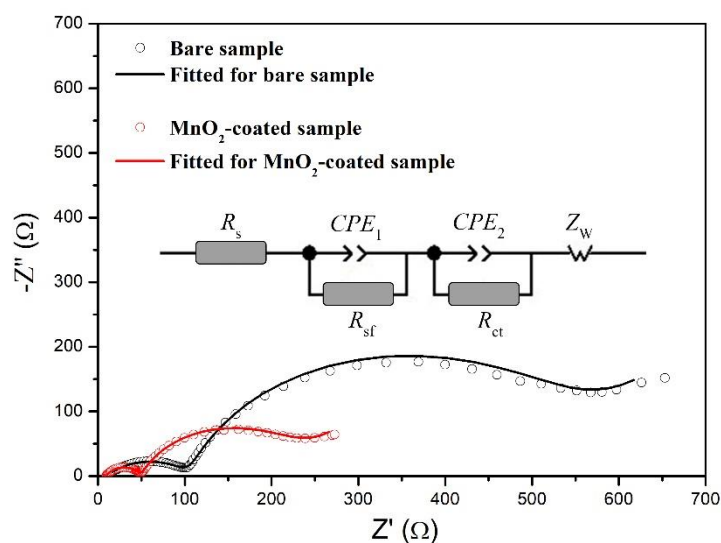


Figure 8. Nyquist plots of the bare and MnO₂-coated LTMO and the equivalent circuit for fitting.

The fitted values of R_s , R_{sf} , and R_{ct} are listed in Table 4. R_s , which contains the impedance of the two electrodes, separator, and electrolyte, showed close values for the two samples. Nonetheless, the values of R_{sf} and R_{ct} for the MnO₂-coated sample were 39.7 and 167.8 Ω, exhibiting values that remarkably declined compared to those of the bare one (94.5 and 422.6 Ω). The side reaction occurring on the cathode surface with the electrolyte was significantly impaired after the MnO₂ modification, leading to a decrease in R_{sf} [42]. Furthermore, the electrochemically active MnO₂ coating layer was conducive to Li⁺ transport [43,44], together with the reduced R_{sf} , which accounted for the decrease in R_{ct} for the coated sample. The EIS results demonstrate that the coated MnO₂ was able to accelerate the transmission kinetics of Li⁺ through the interfacial film and sped up the charge transfer reaction, revealing the origin of the superior electrochemical performance of the MnO₂-coated LTMO.

Table 4. Lattice-fitted values of the parameters according to the equivalent circuit.

Sample	R_s (Ω)	R_{sf} (Ω)	R_{ct} (Ω)
Bare	10.3	94.5	422.6
MnO ₂ -coated	9.6	39.7	167.8

4. Conclusions

In summary, a Li-rich layered cathode material, LTMO, was prepared and then successfully coated with MnO₂. Firstly, the MnO₂ coating layer can inhibit the electrolyte from corroding the LTMO surface and can optimize the formation of SEI. Moreover, lithium ions are reversibly inserted into/extracted from MnO₂, which affords an additional capacity. Compared with the bare LTMO, the MnO₂-coated sample displayed a better first discharge capacity, lower initial irreversible capacity loss, superior cyclic performance, and promoted rate capability. After the MnO₂ coating, the first discharge capacity rose from 224.2 to 239.1 mAh/g, and the initial irreversible capacity loss fell from 78.2 to 46.0 mAh/g. Furthermore, the MnO₂-coated LTMO delivered a cyclic retention of 88.2% after 100 cycles at 0.5 C, which is more competitive than that of the bare LTMO with a value of 71.1%. At a high current density of 2 C, the discharge capacity increased from 100.5 to 136.9 mAh/g after the modification with MnO₂. The EIS results illustrate that the electrochemically active MnO₂ can enhance the transmission kinetics of lithium ions through the interfacial film and can speed up the charge transfer reaction. Therefore, MnO₂ should be a beneficial surface modification material for promoting the electrochemical properties of LTMO.

Author Contributions: Conceptualization, Z.L.; methodology, Z.L.; software, P.Y. and Z.Z.; validation, Z.L.; formal analysis, Z.L.; investigation, Z.L. and P.Y.; resources, Z.L. and Q.P.; data curation, Z.L.; writing—original draft preparation, Z.L. and P.Y.; writing—review and editing, Z.L.; visualization, P.Y.; supervision, Q.P.; project administration, Z.L., Y.L. (Yao Li), and J.X.; funding acquisition, Z.L., Q.P., and Y.L. (Yisi Liu). All authors have read and agreed to the published version of the manuscript.

Funding: This work was financially supported by the National Natural Science Foundation of China (No. 52007054, 51901074, 22008058), Hubei Provincial Natural Science Foundation of China (No. 2020CFB472), and Research Project of Hubei Provincial Department of Education (No. B2020131).

Conflicts of Interest: The authors declare no conflict of interest.

References

- Niu, C.; Liu, D.; Lochala, J.A.; Anderson, C.S.; Cao, X.; Gross, M.E.; Xu, W.; Zhang, J.-G.; Whittingham, M.S.; Xiao, J.; et al. Balancing interfacial reactions to achieve long cycle life in high-energy lithium metal batteries. *Nat. Energy* **2021**, *6*, 723–732. [[CrossRef](#)]
- Ryu, H.-H.; Sun, H.H.; Myung, S.-T.; Yoon, C.S.; Sun, Y.-K. Reducing cobalt from lithium-ion batteries for the electric vehicle era. *Energy Environ. Sci.* **2021**, *14*, 844–852. [[CrossRef](#)]
- Lei, Y.; Ni, J.; Hu, Z.; Wang, Z.; Gui, F.; Li, B.; Ming, P.; Zhang, C.; Elias, Y.; Aurbach, D.; et al. Surface Modification of Li-Rich Mn-Based Layered Oxide Cathodes: Challenges, Materials, Methods, and Characterization. *Adv. Energy Mater.* **2020**, *10*, 2002506. [[CrossRef](#)]
- Li, Y.; Li, Z.; Chen, C.; Yang, K.; Cao, B.; Xu, S.; Yang, N.; Zhao, W.; Chen, H.; Zhang, M.; et al. Recent progress in Li and Mn rich layered oxide cathodes for Li-ion batteries. *J. Energy Chem.* **2021**, *61*, 368–385. [[CrossRef](#)]
- Kim, S.; Kim, C.; Noh, J.-K.; Yu, S.; Kim, S.-J.; Chang, W.; Choi, W.C.; Chung, K.Y.; Cho, B.-W. Synthesis of layered-layered $x\text{Li}_2\text{MnO}_3\text{-(1-x)}\text{LiMO}_2$ (M = Mn, Ni, Co) nanocomposite electrodes materials by mechanochemical process. *J. Power Sources* **2012**, *220*, 422–429. [[CrossRef](#)]
- He, L.; Xu, J.; Han, T.; Han, H.; Wang, Y.; Yang, J.; Wang, J.; Zhu, W.; Zhang, C.; Zhang, Y. SmPO_4 -coated $\text{Li}_{1.2}\text{Mn}_{0.54}\text{Ni}_{0.13}\text{Co}_{0.13}\text{O}_2$ as a cathode material with enhanced cycling stability for lithium ion batteries. *Ceram. Int.* **2017**, *43*, 5267–5273. [[CrossRef](#)]
- He, W.; Guo, W.; Wu, H.; Lin, L.; Liu, Q.; Han, X.; Xie, Q.; Liu, P.; Zheng, H.; Wang, L.; et al. Challenges and Recent Advances in High Capacity Li-Rich Cathode Materials for High Energy Density Lithium-Ion Batteries. *Adv. Mater.* **2021**, 2005937. [[CrossRef](#)]
- Xu, G.; Li, J.; Xue, Q.; Dai, Y.; Zhou, H.; Wang, X.; Kang, F. Elevated electrochemical performance of $(\text{NH}_4)_3\text{AlF}_6$ -coated $0.5\text{Li}_2\text{MnO}_3\text{-}0.5\text{LiNi}_{1/3}\text{Co}_{1/3}\text{Mn}_{1/3}\text{O}_2$ cathode material via a novel wet coating method. *Electrochim. Acta* **2014**, *117*, 41–47. [[CrossRef](#)]
- Zheng, J.; Myeong, S.; Cho, W.; Yan, P.; Xiao, J.; Wang, C.; Cho, J.; Zhang, J.G. Li- and Mn-Rich Cathode Materials: Challenges to Commercialization. *Adv. Energy Mater.* **2016**, *7*, 1601284. [[CrossRef](#)]
- Wang, Z.; Liu, E.; Guo, L.; Shi, C.; He, C.; Li, J.; Zhao, N. Cycle performance improvement of Li-rich layered cathode material $\text{Li}[\text{Li}_{0.2}\text{Mn}_{0.54}\text{Ni}_{0.13}\text{Co}_{0.13}\text{O}_2]$ by ZrO_2 coating. *Surf. Coat. Technol.* **2013**, *235*, 570–576. [[CrossRef](#)]
- Zhou, L.; Wu, Y.; Huang, J.; Fang, X.; Wang, T.; Liu, W.; Wang, Y.; Jin, Y.; Tang, X. Enhanced electrochemical performance of $\text{Li}_{1.2}\text{Mn}_{0.54}\text{Ni}_{0.13}\text{Co}_{0.13}\text{O}_2$ cathode material coated with Li^+ -conductive Li_2SiO_3 for lithium ion batteries. *J. Alloys Compd.* **2017**, *724*, 991–999. [[CrossRef](#)]
- Yabuuchi, N.; Yoshii, K.; Myung, S.T.; Nakai, I.; Komaba, S. Detailed studies of a high-capacity electrode material for rechargeable batteries, $\text{Li}_2\text{MnO}_3\text{-LiCo}_{1/3}\text{Ni}_{1/3}\text{Mn}_{1/3}\text{O}_2$. *J. Am. Chem. Soc.* **2011**, *133*, 4404–4419. [[CrossRef](#)]
- Xiao, Z.; Meng, J.; Li, Q.; Wang, X.; Huang, M.; Liu, Z.; Han, C.; Mai, L. Novel MOF shell-derived surface modification of Li-rich layered oxide cathode for enhanced lithium storage. *Sci. Bull.* **2018**, *63*, 46–53. [[CrossRef](#)]
- Ding, F.; Li, J.; Deng, F.; Xu, G.; Liu, Y.; Yang, K.; Kang, F. Surface Heterostructure Induced by PrPO_4 Modification in $\text{Li}_{1.2}[\text{Mn}_{0.54}\text{Ni}_{0.13}\text{Co}_{0.13}\text{O}_2]$ Cathode Material for High-Performance Lithium-Ion Batteries with Mitigating Voltage Decay. *ACS Appl. Mater. Interfaces* **2017**, *9*, 27936–27945. [[CrossRef](#)] [[PubMed](#)]
- Ma, D.; Li, Y.; Zhang, P.; Cooper, A.J.; Abdelkader, A.M.; Ren, X.; Deng, L. Mesoporous $\text{Li}_{1.2}\text{Mn}_{0.54}\text{Ni}_{0.13}\text{Co}_{0.13}\text{O}_2$ nanotubes for high-performance cathodes in Li-ion batteries. *J. Power Sources* **2016**, *311*, 35–41. [[CrossRef](#)]
- Lou, M.; Zhong, H.; Yu, H.-T.; Fan, S.-S.; Xie, Y.; Yi, T.-F. $\text{Li}_{1.2}\text{Mn}_{0.54}\text{Ni}_{0.13}\text{Co}_{0.13}\text{O}_2$ hollow hierarchical microspheres with enhanced electrochemical performances as cathode material for lithium-ion battery application. *Electrochim. Acta* **2017**, *237*, 217–226. [[CrossRef](#)]
- Deng, B.; Lin, Z.; Chen, Y.; He, W.; Wang, J.; Xie, Q.; Wang, L.; Peng, D.-L. Preparation of porous $\text{Li}_{1.2}\text{Mn}_{0.54}\text{Ni}_{0.13}\text{Co}_{0.13}\text{O}_2$ micro-cubes for high-capacity lithium-ion batteries. *J. Alloys Compd.* **2020**, *834*, 155152. [[CrossRef](#)]
- Lou, M.; Fan, S.-S.; Yu, H.-T.; Xie, Y.; Zhang, Q.; Zhu, Y.-R.; Yi, T.-F.; Tian, G.-H. Mg-doped $\text{Li}_{1.2}\text{Mn}_{0.54}\text{Ni}_{0.13}\text{Co}_{0.13}\text{O}_2$ nano flakes with improved electrochemical performance for lithium-ion battery application. *J. Alloys Compd.* **2018**, *739*, 607–615. [[CrossRef](#)]
- Li, H.; Jian, Z.; Yang, P.; Li, J.; Xing, Y.; Zhang, S. Niobium doping of $\text{Li}_{1.2}\text{Mn}_{0.54}\text{Ni}_{0.13}\text{Co}_{0.13}\text{O}_2$ cathode materials with enhanced structural stability and electrochemical performance. *Ceram. Int.* **2020**, *46*, 23773–23779. [[CrossRef](#)]

20. Xu, L.; Meng, J.; Yang, P.; Xu, H.; Zhang, S. Cesium-doped layered $\text{Li}_{1.2}\text{Mn}_{0.54}\text{Ni}_{0.13}\text{Co}_{0.13}\text{O}_2$ cathodes with enhanced electrochemical performance. *Solid State Ion.* **2021**, *361*, 115551. [[CrossRef](#)]
21. Jafta, C.J.; Ozoemena, K.I.; Mathe, M.K.; Roos, W.D. Synthesis, characterisation and electrochemical intercalation kinetics of nanostructured aluminium-doped $\text{Li}[\text{Li}_{0.2}\text{Mn}_{0.54}\text{Ni}_{0.13}\text{Co}_{0.13}]\text{O}_2$ cathode material for lithium ion battery. *Electrochim. Acta* **2012**, *85*, 411–422. [[CrossRef](#)]
22. Ghorbanzadeh, M.; Allahyari, E.; Riahifar, R.; Hadavi, S.M.M. Effect of Al and Zr co-doping on electrochemical performance of cathode $\text{Li}[\text{Li}_{0.2}\text{Ni}_{0.13}\text{Co}_{0.13}\text{Mn}_{0.54}]\text{O}_2$ for Li-ion battery. *J. Solid State Electrochem.* **2017**, *22*, 1155–1163. [[CrossRef](#)]
23. Wu, Y.; Manthiram, A. High Capacity, Surface-Modified Layered $\text{Li}[\text{Li}_{(1-x)/3}\text{Mn}_{(2-x)/3}\text{Ni}_{x/3}\text{Co}_{x/3}]\text{O}_2$ Cathodes with Low Irreversible Capacity Loss. *Electrochem. Solid-State Lett.* **2006**, *9*, A221–A224. [[CrossRef](#)]
24. Şahan, H.; Göktepe, H.; Patat, Ş.; Yıldız, S.; Özdemir, B.; Ülgen, A.; Mukerjee, S.; Abraham, K.M. Effect of silver coating on electrochemical performance of $0.5\text{Li}_2\text{MnO}_3 \cdot 0.5\text{LiMn}_{1/3}\text{Ni}_{1/3}\text{Co}_{1/3}\text{O}_2$ cathode material for lithium-ion batteries. *J. Solid State Electrochem.* **2019**, *23*, 1593–1604. [[CrossRef](#)]
25. Zheng, J.M.; Li, J.; Zhang, Z.R.; Guo, X.J.; Yang, Y. The effects of TiO_2 coating on the electrochemical performance of $\text{Li}[\text{Li}_{0.2}\text{Mn}_{0.54}\text{Ni}_{0.13}\text{Co}_{0.13}]\text{O}_2$ cathode material for lithium-ion battery. *Solid State Ion.* **2008**, *179*, 1794–1799. [[CrossRef](#)]
26. Wu, Y.; Ming, J.; Zhuo, L.; Yu, Y.; Zhao, F. Simultaneous surface coating and chemical activation of the Li-rich solid solution lithium rechargeable cathode and its improved performance. *Electrochim. Acta* **2013**, *113*, 54–62. [[CrossRef](#)]
27. Shi, S.J.; Tu, J.P.; Tang, Y.Y.; Liu, X.Y.; Zhang, Y.Q.; Wang, X.L.; Gu, C.D. Enhanced cycling stability of $\text{Li}[\text{Li}_{0.2}\text{Mn}_{0.54}\text{Ni}_{0.13}\text{Co}_{0.13}]\text{O}_2$ by surface modification of MgO with melting impregnation method. *Electrochim. Acta* **2013**, *88*, 671–679. [[CrossRef](#)]
28. Kong, J.-Z.; Zhai, H.-F.; Qian, X.; Wang, M.; Wang, Q.-Z.; Li, A.-D.; Li, H.; Zhou, F. Improved electrochemical performance of $\text{Li}_{1.2}\text{Mn}_{0.54}\text{Ni}_{0.13}\text{Co}_{0.13}\text{O}_2$ cathode material coated with ultrathin ZnO. *J. Alloys Compd.* **2017**, *694*, 848–856. [[CrossRef](#)]
29. Li, J.; Li, J.; Yu, T.; Ding, F.; Xu, G.; Li, Z.; Zhao, Y.; Kang, F. Stabilizing the structure and suppressing the voltage decay of $\text{Li}[\text{Li}_{0.2}\text{Mn}_{0.54}\text{Co}_{0.13}\text{Ni}_{0.13}]\text{O}_2$ cathode materials for Li-ion batteries via multifunctional Pr oxide surface modification. *Ceram. Int.* **2016**, *42*, 18620–18630. [[CrossRef](#)]
30. Zhang, S.; Gu, H.; Tang, T.; Du, W.; Gao, M.; Liu, Y.; Jian, D.; Pan, H. In Situ Encapsulation of the Nanoscale Er_2O_3 Phase To Drastically Suppress Voltage Fading and Capacity Degradation of a Li- and Mn-Rich Layered Oxide Cathode for Lithium Ion Batteries. *ACS Appl. Mater. Interfaces* **2017**, *9*, 33863–33875. [[CrossRef](#)] [[PubMed](#)]
31. Li, C.-D.; Yao, Z.-L.; Xu, J.; Tang, P.; Xiong, X. Surface-modified $\text{Li}[\text{Li}_{0.2}\text{Mn}_{0.54}\text{Ni}_{0.13}\text{Co}_{0.13}]\text{O}_2$ nanoparticles with LaF_3 as cathode for Li-ion battery. *Ionics* **2017**, *23*, 549–558. [[CrossRef](#)]
32. Geng, X.; Guo, H.; Wang, C.; Cheng, M.; Li, Y.; Zhang, H.; Huo, H. Surface modification of $\text{Li}_{1.20}\text{Mn}_{0.54}\text{Ni}_{0.13}\text{Co}_{0.13}\text{O}_2$ cathode materials with SmF_3 and the improved electrochemical properties. *J. Mater. Sci.-Mater. Electron.* **2018**, *29*, 19207–19218. [[CrossRef](#)]
33. Chen, D.; Zheng, F.; Li, L.; Chen, M.; Zhong, X.; Li, W.; Lu, L. Effect of Li_3PO_4 coating of layered lithium-rich oxide on electrochemical performance. *J. Power Sources* **2017**, *341*, 147–155. [[CrossRef](#)]
34. Xiao, B.; Wang, B.; Liu, J.; Kaliyappan, K.; Sun, Q.; Liu, Y.; Dadheech, G.; Balogh, M.P.; Yang, L.; Sham, T.-K.; et al. Highly stable $\text{Li}_{1.2}\text{Mn}_{0.54}\text{Co}_{0.13}\text{Ni}_{0.13}\text{O}_2$ enabled by novel atomic layer deposited AlPO_4 coating. *Nano Energy* **2017**, *34*, 120–130. [[CrossRef](#)]
35. Zheng, J.; Deng, S.; Shi, Z.; Xu, H.; Xu, H.; Deng, Y.; Zhang, Z.; Chen, G. The effects of persulfate treatment on the electrochemical properties of $\text{Li}[\text{Li}_{0.2}\text{Mn}_{0.54}\text{Ni}_{0.13}\text{Co}_{0.13}]\text{O}_2$ cathode material. *J. Power Sources* **2013**, *221*, 108–113. [[CrossRef](#)]
36. Xu, G.; Li, J.; Xue, Q.; Ren, X.; Yan, G.; Wang, X.; Kang, F. Enhanced oxygen reducibility of $0.5\text{Li}_2\text{MnO}_3 \cdot 0.5\text{LiNi}_{1/3}\text{Co}_{1/3}\text{Mn}_{1/3}\text{O}_2$ cathode material with mild acid treatment. *J. Power Sources* **2014**, *248*, 894–899. [[CrossRef](#)]
37. Liu, X.; Huang, T.; Yu, A. A new, high energy rechargeable lithium ion battery with a surface-treated $\text{Li}_{1.2}\text{Mn}_{0.54}\text{Ni}_{0.13}\text{Co}_{0.13}\text{O}_2$ cathode and a nano-structured $\text{Li}_4\text{Ti}_5\text{O}_{12}$ anode. *J. Alloys Compd.* **2015**, *648*, 7–12. [[CrossRef](#)]
38. Li, S.; Ji, J.; Li, Z.; Yan, L.; Jiang, W.; Ling, M.; Lin, Z.; Liang, C. Pre-activation and Defects Introduced via Citric Acid to Mitigate Capacity and Voltage Fading in Li-rich Cathode. *Z. Anorg. Allg. Chem.* **2020**, *646*, 1285–1291. [[CrossRef](#)]
39. Zhou, Y.; Cheng, X.; Tynan, B.; Sha, Z.; Huang, F.; Islam, M.S.; Zhang, J.; Rider, A.N.; Dai, L.; Chu, D.; et al. High-performance hierarchical MnO_2/CNT electrode for multifunctional supercapacitors. *Carbon* **2021**, *184*, 504–513. [[CrossRef](#)]
40. Hao, L.; Li, S.-S.; Wang, J.; Tan, Y.; Bai, L.; Liu, A. MnO_2 /multi-walled carbon nanotubes based nanocomposite with enhanced electrocatalytic activity for sensitive amperometric glucose biosensing. *J. Electroanal. Chem.* **2020**, *878*, 114602. [[CrossRef](#)]
41. Huyan, Y.; Chen, J.; Yang, K.; Zhang, Q.; Zhang, B. Tailoring carboxyl tubular carbon nanofibers/ MnO_2 composites for high-performance lithium-ion battery anodes. *J. Am. Ceram. Soc.* **2020**, *104*, 1402–1414. [[CrossRef](#)]
42. Kang, B.J.; Joo, J.-B.; Lee, J.K.; Choi, W. Surface modification of cathodes with nanosized amorphous MnO_2 coating for high-power application in lithium-ion batteries. *J. Electroanal. Chem.* **2014**, *728*, 34–40. [[CrossRef](#)]
43. Wang, B.; Sun, D.; Guo, R.; Liu, Z.; Meng, L.; Zheng, M.; Li, F.; Li, T.; Luo, Y.; Jiang, H. Amorphous MnO_2 -modified $\text{Li}_3\text{V}_2(\text{PO}_4)_3/\text{C}$ as high-performance cathode for LIBs: The double effects of surface coating. *J. Mater. Sci.* **2017**, *53*, 2709–2724. [[CrossRef](#)]
44. Guo, X.; Cong, L.-N.; Zhao, Q.; Tai, L.-H.; Wu, X.-L.; Zhang, J.-P.; Wang, R.-S.; Xie, H.-M.; Sun, L.-Q. Enhancement of electrochemical performance of $\text{LiNi}_{1/3}\text{Co}_{1/3}\text{Mn}_{1/3}\text{O}_2$ by surface modification with MnO_2 . *J. Alloys Compd.* **2015**, *651*, 12–18. [[CrossRef](#)]
45. Liu, B.; Zhang, Z.; Wan, J.; Liu, S. Improved electrochemical properties of YF_3 -coated $\text{Li}_{1.2}\text{Mn}_{0.54}\text{Ni}_{0.13}\text{Co}_{0.13}\text{O}_2$ as cathode for Li-ion batteries. *Ionics* **2017**, *23*, 1365–1374. [[CrossRef](#)]
46. Kong, J.-Z.; Wang, C.-L.; Qian, X.; Tai, G.-A.; Li, A.-D.; Wu, D.; Li, H.; Zhou, F.; Yu, C.; Sun, Y.; et al. Enhanced electrochemical performance of $\text{Li}_{1.2}\text{Mn}_{0.54}\text{Ni}_{0.13}\text{Co}_{0.13}\text{O}_2$ by surface modification with graphene-like lithium-active MoS_2 . *Electrochim. Acta* **2015**, *174*, 542–550. [[CrossRef](#)]